Journal of Applied Fluid Mechanics, Vol. 9, No. 3, pp. 1237-1246, 2016.
Available online at www.jafmonline.net, ISSN 1735-3572, EISSN 1735-3645.
DOI: 10.18869/acadpub.jafm.68.228.22971

CAD Modeling of Store Carrying Rack-9 / Store Carrying Rack-9A, Their Aerodynamic Analysis and Validation through Wind Tunnel Test

A. Bilal† and S. S. Shah

College of Aeronautical Engineering, National University of Sciences and Technology, H-12, Islamabad, Pakistan

†*Corresponding Author Email: ahmed.ixloo@gmail.com*

(Received May 5, 2014; accepted May 20, 2015)

ABSTRACT

Purpose of this research work is to model and analyze the Store Carrying Rack (SCR) of a fighter aircraft with an objective to improve its aerodynamic performance. Refined and grid independent mesh is generated with a technique used for symmetric bodies. The different CFD technique, to capture the flow physics parallel and perpendicular to the wall of the rack, is implemented. It includes capturing the boundary layer, flow separation, vortices formation etc. Results, for the actual flight conditions of the aircraft, are acquired. The results were compared to identify the reason of modification in model. CFD results of racks were validated through Wind Tunnel Test of a scaled down model in a subsonic Wind Tunnel. A new model is proposed having least drag among all the three models. Sears-Hacck volume distribution is the datum for modification in shape. The new proposed model SCR-9AB is recommended for the future shape modification of SCR.

Keywords: Boundary layer; Vortices; Wind Tunnel Analysis; Subsonic Wind Tunnel; Turbulence; Fabrication; Turbulence models, Sears-Hacck Body, Flow rotation, Vorticity.

NOMENCLATURE

A	angle of attack	SCR	store carrying rack
CAD	computer aided design	WTT	wind tunnel test
CFD	computational fluid dynamics	y^+	dimensionless distance to the wall
CMM	coordinates measuring machine	σ	streamline curvature
CNC	computer numerically controlled	ε	dissipation rate
C_{Du}	horizontal buoyancy	$\boldsymbol{\varepsilon_{sb}}$	solid blockage
G-Code	generation code	$\boldsymbol{\varepsilon_{wb}}$	wake blockage
Re	Reynolds number		

1. INTRODUCTION

Store Carrying Rack (SCR) is a component of aircraft that is installed under the wing of aircraft. It can carry three separate payloads on three different stations at a time. The particular rack which is being analysed in this research is capable of carrying payload up to 1000 lbs. on each station thus summing up the total capacity of 3000lbs for SCR. The old model of SCR was named Store Carrying Rack-9. The technological advancements in research and technology have forced the manufacturers to upgrade the shape of the model. So a modified shape of the model is designed and manufactured that is known as Store Carrying Rack-9A.

The new shape of the SCR is more aerodynamic and its avionics system is also upgraded. This research work includes only the aerodynamic study of the SCRs. The flow properties will be enhanced by the new SCR-9A as compared to SCR -9.

The rack is studied in order to identify the basic reason of modification in shape of the model. The aerodynamic analysis to calculate the aerodynamic parameters is part of the research. The comparison of those parameters prognosticates that what are the enhanced properties and thus proposes the manufacturing modifications.

Researches using CFD techniques must have validation of the results of the analysis. The validation tells the accurateness of the CFD results. Wind tunnel testing technique is used in this

research for validation purpose. (Pope *et al*. 1999)

2. CAD MODELLING

For CFD the most important part is the CAD model. The model is required for the purpose of meshing. For an accurate CAD modelling, correct data point information is required to be plotted in the software. The data point data is collected from the original model under analysis. (CHAOQUN *et al* 2006)

CMM machines are used for the acquisition of coordinates of any model and that traced data is plotted to obtain the CAD model. For this research work the methodology incorporated is to get the coordinates by the Laser CMM. For this purpose the whole model of SCR was meshed and then the coordinates were measured using the Laser CMM. The technique employed in this was to keep the x coordinates constant and make contours from y and z coordinates. This will help in obtaining curves that can be protruded. This is the basic technique of obtaining a CAD model from the point clouds or data points.

The data points were imported in the software and then were used to make curves. The curves look like as shown in "Fig 1."

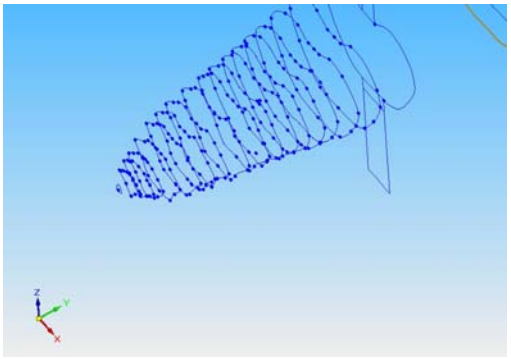

Fig. 1. Curves from Data Points.

These curves can easily be loft protruded. The lofted protrusion goes along with the defined path and creates a smooth body joining all that curves. Thus a smooth body is created by this method. The final shape obtained using this method is shown in "Fig 2."

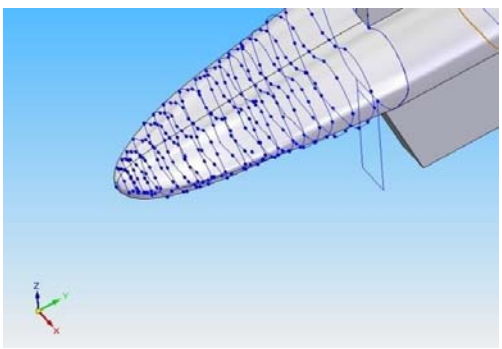

Fig. 2. Lofted Protruded Body.

By this method the final shape of the CAD model of both the racks are presented in "Fig 3" and "Fig 4".

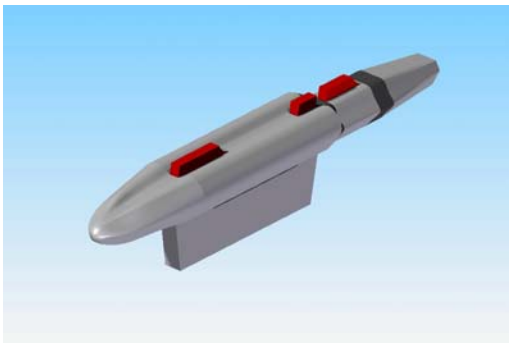

Fig. 3. SCR-9.

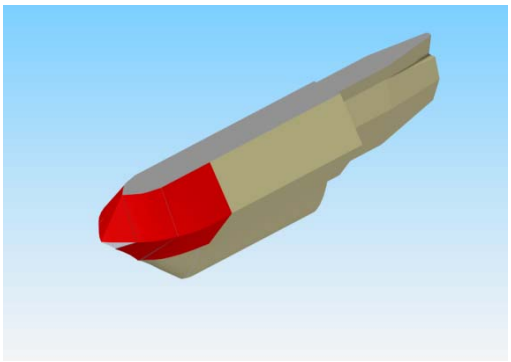

Fig. 4. SCR-9A.

3. MESHING

Since the computer recognizes only numbers, we have to translate our geometrical and mathematical models into numbers. This process is called discretization. The process of grid generation is in general complex and requires dedicated software tools to help in defining grids that follow the solid surfaces. (ICEM Theory Guide)

The results of a CFD simulation and its accuracy dependents on the grid properties and quality (FLUENT Theory Guide). Once a grid is available, we can initiate the second branch of the discretization process, namely the discretization of the mathematical model equations. (ICEM Theory Guide)

The purpose of meshing is to decompose the solution domain into an appropriate number of locations for an accurate result. A mesh divides geometry into many elements. These are used by the CFD solver to construct control volumes.

More elements require more computational resource (memory and processing time). Balance is usually required while performing the mesh optimization. This type of balance is known as Grid independence. It is very substantial procedure and forms up the base for solution initialization. (Gerasimov 2006)

After SCRs CAD modeling, the geometries were imported in meshing software and then meshing parameters were defined. Due to complex geometry, unstructured mesh was grown with the

patch independent scheme of ANSYS®. For mesh in volume robust octree scheme was used. Above mentioned configuration works well with the complex geometries, so it is used in our case. (ICEM Theory Guide)

A structured grid, for capturing the boundary layer region over the SCR, was used while an unstructured grid was used for the rest of the domain (Cheah *et al.* 2009). Unstructured meshing was selected because the flow parameter of interest, such as pressure variation, lift and drag, do not require a very fine mapped mesh. This scheme of meshing, used for the boundary layer capturing, is called prism layer formation. ANSYS® software is used for this purpose. (FLUENT Theory Guide)

A technique incorporated in the research work is to cut down the object on the symmetry plane and then mesh that domain. After the results, the rack was mirrored on the symmetry plane. This technique limits the mesh to half domain as compared to the full domain and thus helps in reducing the mesh. This helps saving the computational time and computational capability requirement is also reduced as well. It is very useful technique used for the CFD of symmetric cases. This is shown in the "Fig 5."

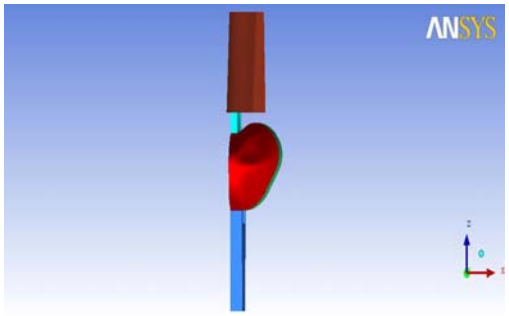

Fig. 5. Cut down on symmetry plane.

Some of the meshing techniques used include the tetra width ratio of ANSYS (ICEM Theory Guide). It creates very fine mesh closer to the body of the object and increases the size of mesh with ratio mentioned in the tetra width ratio box. So it reduces the mesh and thus saves computational power required for CFD simulation. This can be viewed in the volume mesh as shown in Fig.6

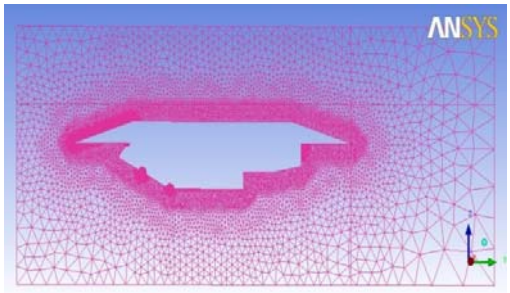

Fig. 6. Tetra width ratio.

Another technique used in the meshing is the curvature and proximity based refinement of the mesh (ICEM Theory Guide). Curvature/Proximity Based Refinement when enabled, the mesh is automatically refined based on geometry curvature and proximity. This will result in larger elements on flat planar surfaces and smaller elements in areas of high curvature or within small gaps. (Cheah *et al.* 2009)

Meshing parameters were defined and mesh was generated. This mesh formed was of smaller size near to the rack body and larger size in the rest of domain. This is required in order to capture flow accurately near to rack body and while rest domain flow can modeled with larger size mesh. The volume mesh and meshed domain obtained using the above techniques and parameters are shown in "Fig .7" and "Fig.8".

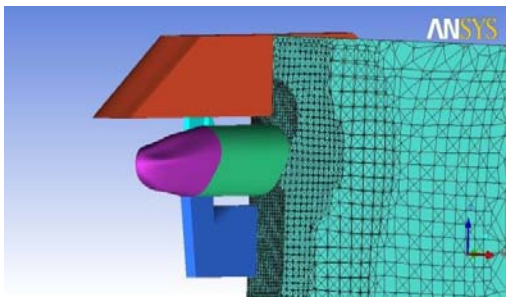

Fig. 7. Volume mesh.

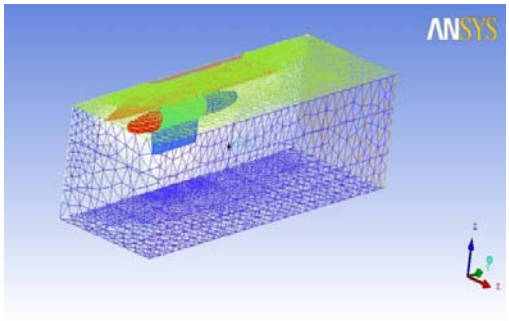

Fig. 8. Meshed domain.

Grid independence test was carried out to get a solution independent of the grid (Cheah *et al.* 2009). For that a sequence of simulations was carried out and results were obtained as shown in Table 1 and Table 2.

Table 1 SCR-9 Grid independence test

Model	**1206098**	**2591066**	**2856635**
C_L	**0.00768**	**0.00815**	**0.00816**
C_D	**0.00051**	**0.00062**	**0.00063**

Table 2 SCR-9A grid independence test

Model	**1166589**	**1974167**	**2246851**
C_L	0.00589	0.00604	0.00606
C_D	0.00228	0.00231	0.00232

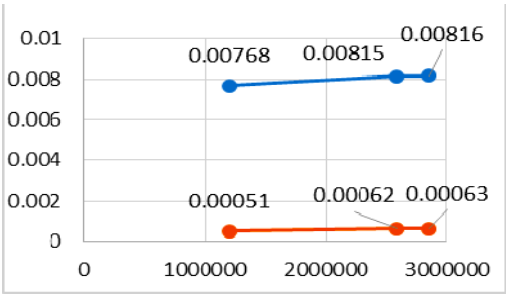

Fig. 9. SCR-9 Results for grid independence test.

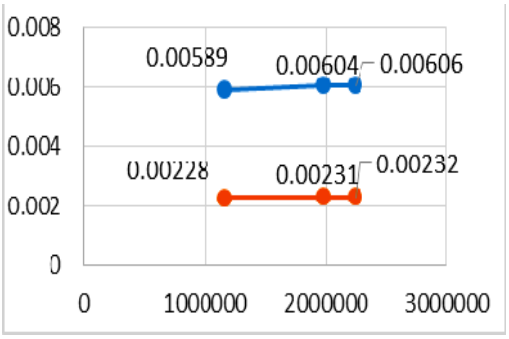

Fig. 10. Results for SCR-9A grid independence test.

So the optimum grid size obtained by the grid independence study is shown in "Table 3".

Table 3 Grid independence study

Model	Nodes	Elements
TER-9	456057	2591066
TER-9A	345220	1974167

4. CFD RESULTS

CFD simulation results are the pith of CFD research (Moser *et al.* 1987). Parameters for CFD simulation were defined and the boundary conditions were set according to the flight conditions of aircraft. The turbulence model is the first thing to be decided that depend on the mesh of the model. For this reason, for all further analysis k- ε (realizable) turbulence model is used (CHOW *et al.* 2005). The reason is that S-A model does not provide very good results for coarse meshes since it is originally a low-Reynolds number solver. k- ω (SST) is also not used because of its demand of very low y^+ value that is ≈1 range. So we cannot achieve this value for the restricted range of mesh size. Furthermore, k- ε (realizable) accurately predicts the spreading of round and planar jets, improved performance for streamline curvature, rotation and vortices. So it is decided to use the k- ε (realizable) (CHOW *et al.* 2005).

Explicit formulation, for the temporal discretization, and first order upwind scheme, for the spatial discretization, is used. A fine, grid independent mesh, was selected for the final simulation and results calculation (Carlson 1998). Boundary wall types of domain were defined as pressure outlet except inlet and roof. This is done to simulate actual flow condition for the case. (FLUENT User guide)

The results obtained are shown in the Fig.11 and "Fig 12".

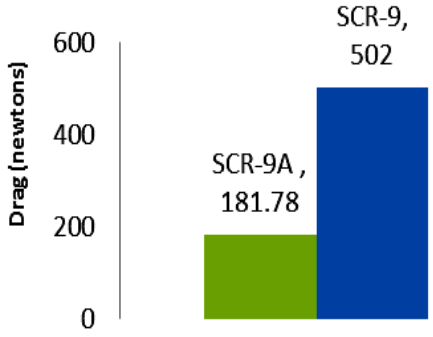

Fig. 11. Drag comparison of racks.

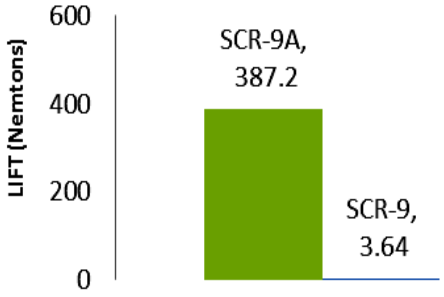

Fig. 12. Lift comparison of racks.

This shows the significant changes in the lift and drag forces of the STORE CARRYING RACK-9 and STORE CARRYING RACK-9A models. This comparison bars avow clearly the reason of modification that the new model is improved for obtaining better values of both the aerodynamic parameters LIFT and DRAG.

Some of the special properties of the flow captured by CFD due to very fine mesh are

- Flow separation
- Boundary layer capture
- Eddies formation
- Vortices
- Wake region
- Path lines
- Rotation

Fig.13 represents the boundary layer captured due to the fine mesh.

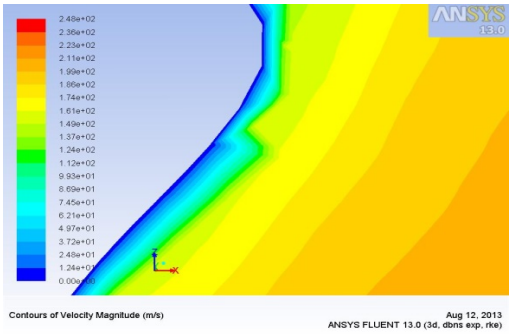

Fig. 13. Boundary layer captured.

The cell height and turbulence model selection have captured the flow perpendicular to the wall. (CHAOQUN *et al.* 2006)

The wake region formation and the vortices formation behind the body is captured well by the mesh. It is shown in Fig.14 that flow separates at the rear of the body forming vortices. Similarly the Fig.15, Fig.16 and Fig.17 also capture the similar behavior of flow. (FLUENT User guide)

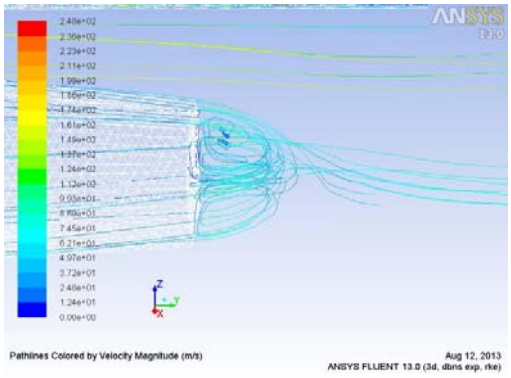

Fig. 14. Path lines depicting vortices.

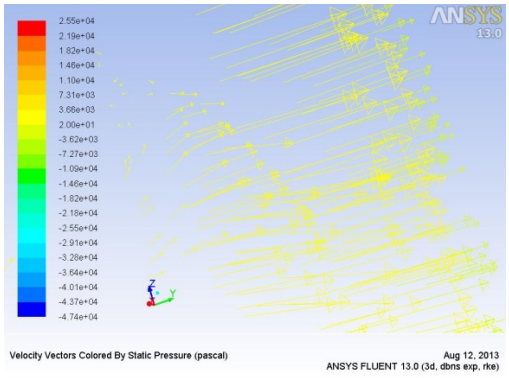

Fig. 15. Flow vectors showing rotation.

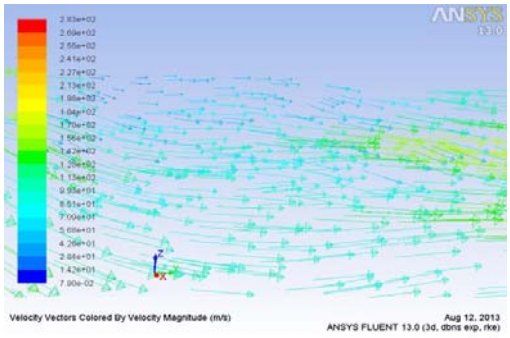

Fig. 16. Wake region.

The pressure contours over the body of SCRs shows the location of high aerodynamic loads. The SCR-9A loads shows that it is more aerodynamic as compared to SCR-9 as pressure is not increasing abruptly. So the pressure drag is lower for SCR-9A as compared to SCR-9 that is the major factor of aerodynamic drag in blunt bodies (FLUENT User guide). The representations of above are in Fig.18 and "Fig.19".

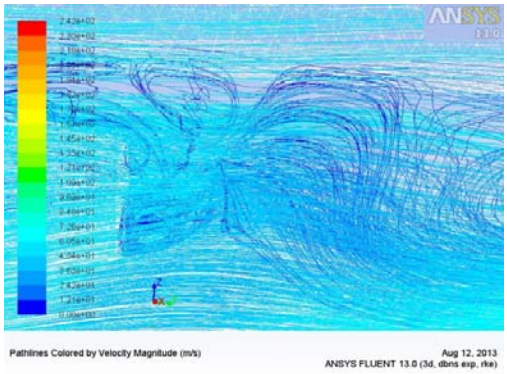

Fig. 17. Flow rotation.

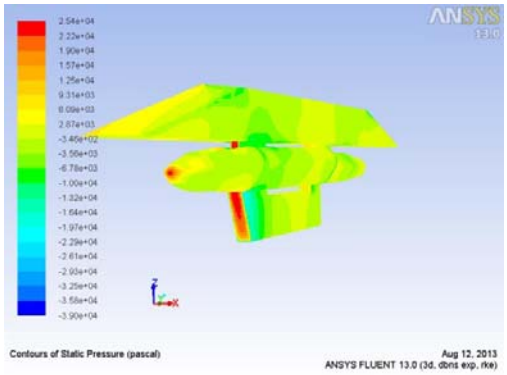

Fig. 18. Pressure distribution SCR-9.

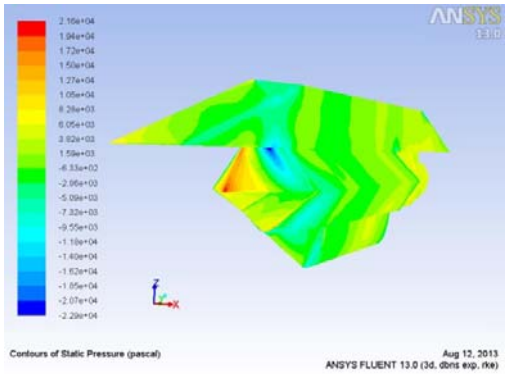

Fig. 19. Pressure distribution SCR-9A.

5. VERIFICATION OF TURBULENCE MODEL

y+ of the mesh is the major player in deciding the turbulence model of the CFD (FLUENT User guide). As the Fig.20 is clearly depicting that y+ is lying in 30 to 90 so that is the ideal range for the selection of k-ε (realizable). So the turbulence model incorporated is the k-epsilon mode (CHEAH *et al.* 2009) (BEHNIA *et al.* 2003) (CHOW *et al.* 2005). So the verification, of using correct turbulence model with the mesh, is done.

6. EXPERIMENTAL VALIDATION

The experimental validation of the CFD result is a coercion. By this the error in the CFD results can be determined or deviation from the actual values can be sought. (Bushnell 2006).

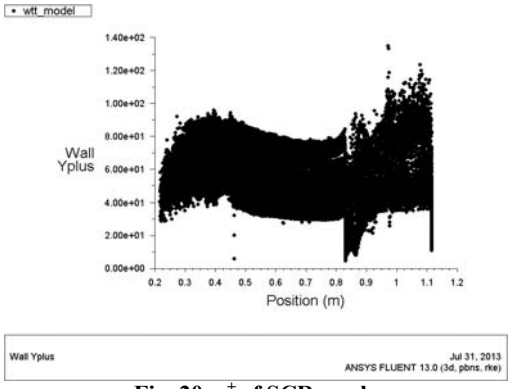

Fig. 20. y^+ of SCR mesh.

6.1 G-Coding and Fabrication

For the fabrication SCR-9A was selected due to ease in fabrication for its simpler shape compared to the shape and contours of SCR-9.

For the G- code generation, the CAD model is imported to the software. The G- code converts the machining operation into the machine language. It also auto-selects tool for the cutting purpose. For the model of rack tools used were end mill cutter, ball mill and bull mill (Bilal *et al.* 2013)

Once the code is generated then comes the selection of material for fabrication and scale selection which depends upon the capacity of the wind tunnel test section. For material the cost effective model was sought (Bushnell 2006). The least cost material available and used in test of wind tunnel is wood. So seesham wood was selected and the half scale down model was decided for test keeping in view the capacity of the wind tunnel test section that is 2x3 ft. cross section with 6 ft. length shown in"Fig.21".

The final shape of the fabricated model of the rack was achieved after continuous machining of 24 hours on CNC lathe including 10 hours for surface finishing operation. The final shape obtained is shown in Fig.22. (Bilal *et al.* 2013)

Fig. 21. Wind tunnel test section.

Fig. 22. SCR-9A scaled down model.

6.2 Wind Tunnel Testing

After the calibration of balance of wind tunnel was done the model was mounted on the supports of the wind tunnel. The speeds selected for the test were

- 90 mph(132 ft./s) (Mach 0.11)
- 120mph(176 ft./s) (Mach 0.15)
- 140 mph(205.33 ft./s) (Mach 0.18)
- 160mph(234.66 ft./s) (Mach 0.21)

On these speeds the wind tunnel test were conducted with 4 values of α. The values were 0°, 3°, 6° and 8°.

The correction factors for the wind tunnel test are

- Balance Alignment Correction Factor
- Tare and Interference Drag
- Wind Tunnel Boundary Corrections
- Solid Blockage ε_{sb}
- Wake Blockage ε_{wb}
- Horizontal Buoyancy C_{Du}
- Streamline curvature σ (Bushnell 2006) (Bilal *et al.* 2013)

These values were calculated and the correction factors were applied before the final result. The values of correction factors are given as in Table 4 and Table 5.

Table 4 Correction Factors

σ	ε_{sb}	ε_{wb}	ε
0.447	0.194	0.006	0.201

Table 5 Horizontal Buoyancy

α (radians)	C_{Du}
0.00000	0.01806
0.05236	0.04036
0.10472	0.05396
0.13963	0.05635

CFD for the racks are done for zero degree α configuration only. A scaled down CAD model was assigned the actual boundary condition of WTT and two turbulence models were used for the problem solution. They are SA and k-ε (realizable). The results were compared for α=0°. The results are shown below in Table 6. Drag is the parameter selected for the comparison of the results of CFD and WTT.

Table 6 WTT results at α=0°

WTT Speeds	C_D
90mph	0.00726
120mph	0.01016
140mph	0.01048
160mph	0.01064

Results for the CFD of two turbulence models, SA and k-ε (realizable), are shown in Table 7.

Table 7 CFD results at α=0°

Speeds	Model	C_d
90	SA	0.01713
	k-ε (realizable)	0.005666
120	SA	0.009899
	k-ε (realizable)	0.01214
140	SA	0.01128
	k-ε (realizable)	0.009388
160	SA	0.01117
	k-ε (realizable)	0.009135

6.3 Comparison

The comparison of the results obtained by CFD and WTT is done in "Fig. 23".

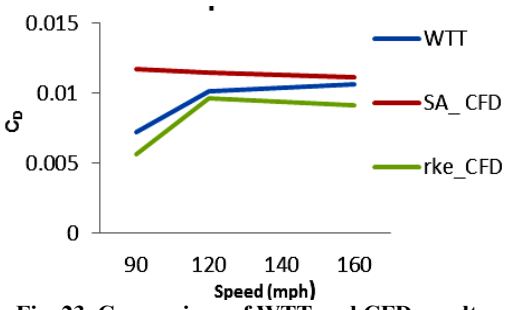

Fig. 23. Comparison of WTT and CFD results.

The comparison shows that the k-ε (realizable) is giving more accuracy in results as compared to the SA model results. This comparison shows that the k-ε (realizable) is more accurate than SA so that is why we can use it for the analysis of the complex geometries and where the boundary layer calculation is of secondary importance. (CHOW *et al.* 2005)

The k-ε (realizable) model can capture the boundary layer, vortices, rotation and complex secondary properties of flow quite well as compared to the SA model so for complex geometry especially in transonic and supersonic regime it is advised to use this model. (CHOW *et al.* 2005)

Our CFD results are very close to the experimental results so that is why it is firmly concluded that the CFD of the model is correct.

The wind tunnel test was also carried out for different configurations of speeds as well as α. The results for the configuration of speed as 90mph is shown in Table 8.

Table 8 Results for 90mph

α(degree)	C_L	C_D
0	0.00319	0.00726
3	0.00460	0.01556
6	0.00565	0.02027
8	0.00566	0.02107

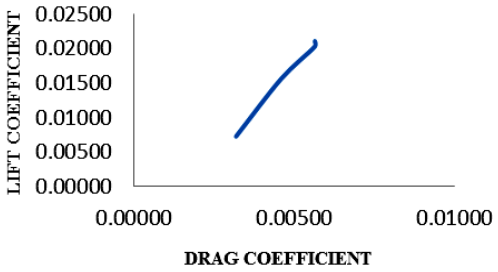

Fig. 24. L/D curve at 90 mph.

Similarly the values for the next three configurations of speeds are shown in Table 9, 10 and 11.

Table 9 Results for 120mph

α (degree)	C_L	C_D
0	0.00265	0.01016
3	0.00495	0.01248
6	0.00607	0.01619
8	0.00638	0.01736

Table 10 Results for 140mph

α (degree)	C_L	C_D
0	0.00294	0.01042
3	0.00469	0.01525
6	0.00640	0.01675
8	0.00705	0.01683

Table 11 Results for 160mph

α (degree)	C_L	C_D
0	0.00255	0.01064
3	0.00410	0.01238
6	0.00538	0.01345
8	0.00637	0.01494

So the comparison curves for lift and drag with respect to α at different speeds are shown in "Fig 25 and 26".

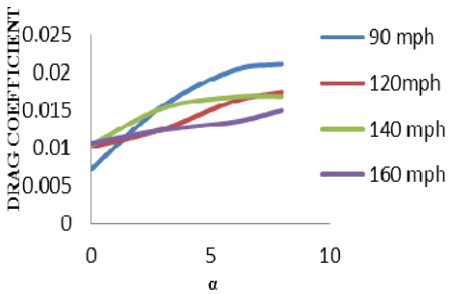

Fig. 25. Drag comparison curve.

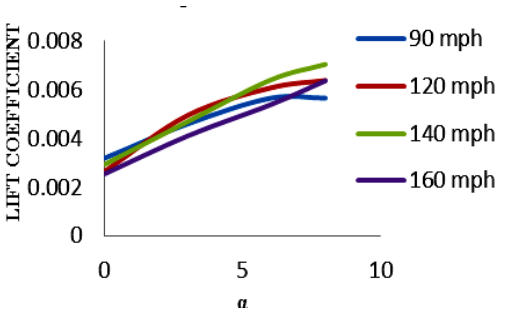

Fig. 26. Lift comparison curve.

6.4 Conclusion on Wind Tunnel Testing

The curves plotted for the particular speed shows that as α is increased the lift and drag value increases. This is indication of the fact that SCR-9A is a good aerodynamic-shaped body with its lift increasing with α. So when installed under the wing of the aircraft it will support the forces of wing. (Bilal *et al.* 2013)

The L/D curve shows that it is in perfect accordance with the aerodynamic bodies so the interference of forces of rack with that of wing force will be positive (Bushnell 2006) i.e. rack aerodynamic forces support the aerodynamic forces of wing. The drag polar will be further supported by the rack forces.

The curve for $\alpha=0^{o}$ is plotted against different speeds and compared as shown in Fig. 27.

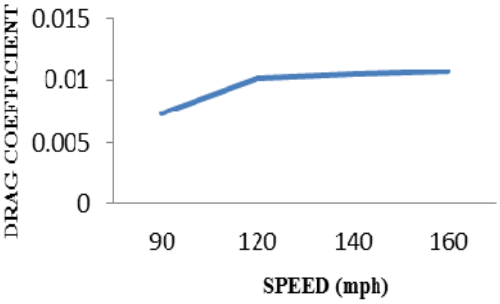

Fig. 27. Comparison of drag at 0º.

This shows that at very low Mach no the flow is attached to the rack body and thus pressure drag value is less but as the speed is increased the flow separation causes a large value of drag that is indicated by Fig.27 (Blackwell 1969).

7. GEOMETRY OPTIMIZATION

Keeping in view the latest design optimization for the aerodynamic bodies in world, need arises to design a more aerodynamic shape of SCR. Usually the SEARS HACCK body design is used to achieve minimum drag design. SCR was modified to achieve a shape that has minimum drag keeping in view the Sears Hacck body as our datum. For this purpose to obtain aerodynamic SCR shape, a volume distribution shown below in "Fig.28" was imitated.

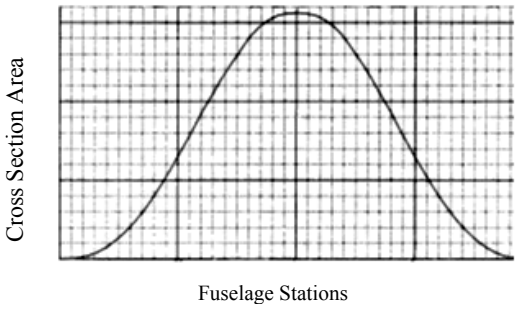

Fig. 28. Sears Hacck body volume distribution.

For obtaining such a volume distribution of the SCR some of the operation as

- Chamfering
- Filleting
- Rounding of edges

By these operations, the models of SCR were modified and proposed. The shapes obtained are as shown in Fig.29 and 30.

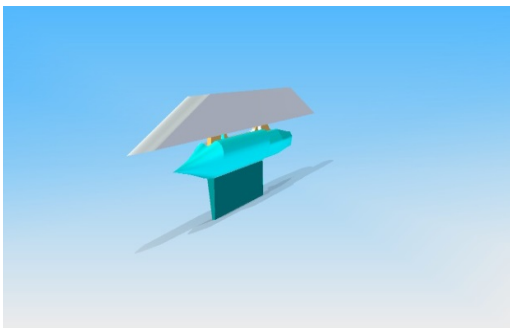

Fig. 29. SCR-9S.

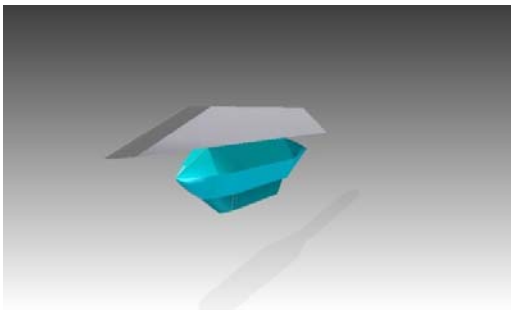

Fig. 30. SCR-9AB.

The comparison of CAD models clearly shows the differences exists between the two modified models are

- Nose cone made round
- Lower part made round, and its edges chamfered
- Rear part is prolonged and sharp edges removed

All these changes are made in order to get the Sears Hack Body approximation for SCR. The body as shown clearly incorporates the approximation in its shape.

7.1 CFD Results

After the CAD modelling of SCR modified models, the grid independent meshes were analyzed under the actual flight conditions. For setup, the turbulence model used was k- ε (realizable). The results obtained are shown in "Table 12".

Table 12 CFD Results

	SCR-9S	SCR-9AB
LIFT (N)	46.82	340.9
DRAG (N)	260.01	181.72

7.2 Comparison

The comparison of CFD results shows, in "Fig.31, that the model of SCR-9AB proposed is the best in all four models and can be selected for the future modification and manufacturing. The Sears Hack Body approximation on the model has not only reduced the drag force but also increased its lift value. So it is proposed for the modification in design of SCR.

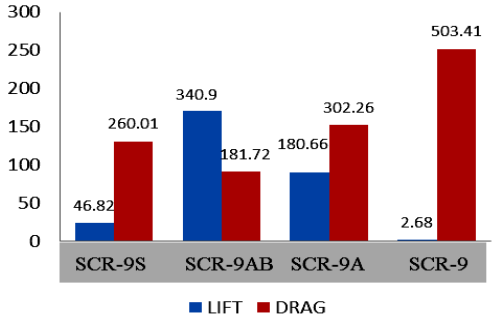

Fig. 31. Comparison of CFD results.

8. Conclusions and Recommendations

This research study clearly aggrandizes previous studies that for complex flow properties the k-ε (realizable) is more reliable as compared to the SA model. The reason being its modified equation for epsilon can capture vortices, rotation and also its standard function to capture the log-law region makes it quite accurate. This cogent argument comes from the results of wind tunnel test.

The model of SCR is changed because of the results of CFD as shown in comparison that its results for lift and drag for STORE CARRYING RACK-9A are much improved as compared to STORE CARRYING RACK-9. The commensurate results are in accordance with the shape of the racks. This research has persuaded the manufacturers to change the aerodynamic shape of SCR.

The new proposed STORE CARRYING RACK-9AB has least drag as given by the CFD results. This is the approximate shape obtained by convoluting the Sears-Hacck body volume distribution to that of SCR. This model is proposed for the future shape modification as eclectic option.

Wind tunnel data have helped CFD development tremendously during last four decades. Through continuous CFD validation of more and more challenging problems using wind tunnel data, confidence in CFD grows and so does the demand on the quality of wind tunnel tests. The congruity test of CFD results with WTT is a coercion. The research can also be done to, use CFD, help wind tunnel tests in respect of wall interference assessment and corrections, especially for the important transonic range, most relevant for current generation.

The early flow separation predicted in WTT is a proof of the fact that sears hacck approximation of the body of the rack can help in the delayed flow separation. This will reduce the pressure drag value and thus curbing the parasitic drag of the aircraft.

The diagram shows how CFD can be used for the tunnel corrections. This shows hoe the errors can be embedded in the wind tunnel calculations and thus the wind tunnel corrections can be made as well.

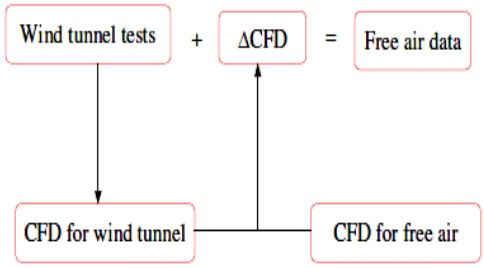

Fig. 32. CFD Correction for wind tunnel data.

References

ANSYS® (2015), Fluent Theory Guide

ANSYS® (2015), ICEM Theory Guide

ARIFF, M., S. M. SALIM and S. C. CHEAH (2009). Wall Y+ Approach for Dealing with Turbulent Flow over a Surface Mounted Cube: Part 2 – High Reynolds number. *Proceedings of. Int. Conf. on CFD in the Minerals and Process Industries*, CSIRO, Melbourne, Australia, December.

Barlow, J. B., W. H. Rae and A. Pope (1999). *Low-Speed Wind Tunnel Testing*. Wiley-Interscience, 3 edition.

Bilal, A., T. A. Shams, F. Akram, A. A. Khan and R. Riaz (2013). Wind Tunnel Testing Of A Scaled Down Model Of Store Carrying Rack In Low Subsonic Wind Tunnel. *International Conference of Modeling and Simulation*, Islamabad, Pakistan.

Blackwell, J. A. (1969). Preliminary study of effects of Reynolds number and boundary-layer transition location on shock-induced separation. Langley Research Center Langley station, Hampton, NASA.

Bushnell, D. M. (2006). Scaling: Wind tunnel to

flight. *Annual Review of Fluid Mechanics* 38, 111–128

Carlson J. R. (1998). Prediction of very high Reynolds number compressible skin friction. *20th AIAA Advanced Measurement and Ground Testing Technology Conference*, Albuquerque, New Mexico

FLUENT, *Documentation: User guide*, ANSYS Inc.

GAO, Y. and W. K. CHOW (2005). Numerical studies on air flow around a cube. *Journal of Wind Engineering and Industrial Aerodynamics* 115-135

GERASIMOV, A. (2006). Modeling Turbulence Flows with Fluent, Europe ANSYS Inc.

IACCARINO, G., A. OOI and M. BEHNIA (2003). Reynolds averaged simulation of unsteady separated flow. *International Journal of Heat and Fluid Flow* 147-156

JINYUAN, T., H. Y. GUAN and L. CHAOQUN (2006). *Computational Fluid Dynamics: A Practical Approach, USA: Butter-Heinemann*

KIM, J., P. MOIN and R. MOSER (1987). Turbulence statistics in fully developed channel flow at low Reynolds number. *Journal of Fluid Mechanics* 133-166

QIN, N. (2003). CFD for Better Understanding of Wind Tunnel Tests. *Integrating Experiments and CFD*, Glasgow